

Chemical controls on fault behavior: Weakening of serpentinite sheared against quartz-bearing rocks and its significance for fault creep in the San Andreas system

Diane E. Moore¹ and David A. Lockner¹

Received 24 September 2012; revised 6 February 2013; accepted 21 February 2013.

[1] The serpentinitized ultramafic rocks found in many plate-tectonic settings commonly are juxtaposed against crustal rocks along faults, and the chemical contrast between the rock types potentially could influence the mechanical behavior of such faults. To investigate this possibility, we conducted triaxial experiments under hydrothermal conditions (200–350°C), shearing serpentinite gouge between forcing blocks of granite or quartzite. In an ultramafic chemical environment, the coefficient of friction, μ , of lizardite and antigorite serpentinite is 0.5–0.6, and μ increases with increasing temperature over the tested range. However, when either lizardite or antigorite serpentinite is sheared against granite or quartzite, strength is reduced to $\mu \sim 0.3$, with the greatest strength reductions at the highest temperatures (temperature weakening) and slowest shearing rates (velocity strengthening). The weakening is attributed to a solution-transfer process that is promoted by the enhanced solubility of serpentine in pore fluids whose chemistry has been modified by interaction with the quartzose wall rocks. The operation of this process will promote aseismic slip (creep) along serpentinite-bearing crustal faults at otherwise seismogenic depths. During short-term experiments, serpentine minerals reprecipitate in low-stress areas, whereas in longer experiments, new Mg-rich phyllosilicates crystallize in response to metasomatic exchanges across the serpentinite-crustal rock contact. Long-term shear of serpentinite against crustal rocks will cause the metasomatic mineral assemblages, which may include extremely weak minerals such as saponite or talc, to play an increasingly important role in the mechanical behavior of the fault. Our results may explain the distribution of creep on faults in the San Andreas system.

Citation: Moore, D. E., and D. A. Lockner (2013), Chemical controls on fault behavior: Weakening of serpentinite sheared against quartz-bearing rocks and its significance for fault creep in the San Andreas system, *J. Geophys. Res. Solid Earth*, 118, doi:10.1002/jgrb.50140.

1. Introduction

[2] The noted association of outcrops of serpentinite with creeping faults of the San Andreas system in central and northern California [e.g., Allen, 1968; Hanna *et al.*, 1972; Irwin and Barnes, 1975] is what initially led us to investigate the frictional properties of serpentinite [Moore *et al.*, 1996b, 1997], extending the work of Reinen *et al.* [1991, 1992, 1994] to elevated temperatures. These experiments demonstrated that the serpentine minerals have the potential to slide unstably under certain conditions (velocity-weakening behavior), apparently making it unlikely that serpentinite could be the cause of fault creep. The serpentine varieties lizardite and antigorite are also among the stronger phyllosilicate minerals and so could not explain the very low strength of

the central creeping section of the San Andreas fault inferred from stress orientation and heat-flow investigations [e.g., Chéry *et al.*, 2004; Fulton *et al.*, 2004; Hickman and Zoback, 2004; Williams *et al.*, 2004]. Even chrysotile, which is very weak at temperatures up to $\sim 100^\circ\text{C}$ [Reinen *et al.*, 1994; Reinen and Tullis, 1995; Moore *et al.*, 1996b], becomes substantially stronger and is largely velocity weakening at higher temperatures [Moore *et al.*, 2004]. More extreme P - T conditions, such as those in the deeper portions of subduction zones (1–1.5 GPa pressure, temperatures to 700°C), are required to substantially weaken and stabilize shear of antigorite [Chernak and Hirth, 2010].

[3] The experiments described above tested the behavior of serpentinite in an ultramafic chemical system, that is, shear of serpentinite against or between serpentinite and other ultramafic rocks. However, serpentinites commonly are juxtaposed against crustal rocks at depth along faults. Numerous field studies have shown that ultramafic and crustal rocks are chemically incompatible, characterized in the long term by the development of reaction zones at the contact between them [e.g., Coleman, 1967; Koons, 1981;

¹U. S. Geological Survey, Menlo Park, California, USA.

Corresponding author: D. E. Moore, U. S. Geological Survey, Menlo Park, CA 94025, USA. (ore@usgs.gov)

This paper is not subject to U.S. copyright.
Published in 2013 by the American Geophysical Union.
2169-9313/13/10.1002/jgrb.50140

Sanford, 1982; Mori et al., 2007]. How might this incompatibility affect the mechanical behavior of serpentinite?

[4] To address this question, we conducted a laboratory investigation in which serpentinite gouges were sheared between driving blocks of quartz-rich crustal rocks under hydrothermal conditions (200–350°C). We reported the results of a reconnaissance study in *Moore et al. [2010]* and describe a new set of experiments in this paper. The strengths of lizardite and antigorite serpentinite decrease markedly with increasing temperature (temperature weakening) and decreasing shearing rate (velocity strengthening) when sheared against quartzose rocks, thus promoting aseismic slip and weakening at P - T conditions that normally correspond to the seismogenic zone of crustal faults. We discuss the implications of these data for the behavior of continental fault zones, with particular emphasis on the San Andreas system of central and northern California. It should be emphasized, however, that our findings also apply to other plate-tectonic settings, including subduction zones and oceanic detachment and transform faults. Those faulting environments will be considered in a separate paper that will also include the results of equivalent experiments on fresh ultramafic rocks.

2. Experiments Conducted

2.1. Gouge and Rock Materials Tested

[5] For all of the experiments reported in this study, a thin layer of synthetic fault gouge was sheared between rock driving blocks (Table 1). In most cases the gouge layer was antigorite- or lizardite-rich serpentinite and the driving blocks either Westerly granite or quartzite. Two additional experiments were run with a gouge of chrysotile serpentinite. These gouge samples came from the same stocks that we used in previous studies [e.g., *Moore et al., 1997, 2004; Moore and Lockner, 2007*]. Control experiments involved shear of the three serpentinite gouges between driving blocks of antigorite serpentinite, and shear of quartz and granite

gouges between driving blocks of quartzite and Westerly granite, respectively (Table 1).

2.1.1. Serpentinite Starting Materials

[6] Both the antigorite gouge and the serpentinite driving blocks were prepared from boulders of antigorite-rich serpentinite collected at the KCAC, Inc. asbestos mine near New Idria, California. The rock specimens used to prepare the gouge contain approximately 75% by volume serpentinite, with ~12% magnetite and ~8% calcite. Minor amounts of chlorite, brucite, spinel, and sulfides are also present. To prepare the gouge, pale-green veins of chrysotile \pm calcite were removed before manually grinding the sample and passing it through a 90 μ m sieve. Antigorite is the only serpentinite mineral to appear in bulk X-ray diffraction (XRD) patterns of the prepared gouge. Based on microprobe analyses [*Moore et al., 1996a*], the antigorite contains 2–2.5 wt% Al_2O_3 , ~4.5 wt% FeO (total Fe reported as FeO), and 0.5 wt% Cr_2O_3 .

[7] The lizardite serpentinite, collected at Gold Beach, Oregon, contains more than 90% by volume serpentinite, and lizardite 1T is the only serpentinite variety identified by powder XRD analysis. The composition of the lizardite varies with its occurrence. The cores of mesh-texture lizardite (after olivine) contain ~2.2 wt% Al_2O_3 and ~8 wt% FeO, and the rims have ~0.6 wt% Al_2O_3 and 4 wt% FeO. The less abundant bastite-texture lizardite (after pyroxene) contains 3.5–5 wt% Al_2O_3 and 7–8 wt% FeO. Magnetite is the chief accessory mineral at ~5%, and minor to trace amounts of spinel, chlorite, ilmenite, and Mn-oxide are also present. As with the antigorite serpentinite, pale-green veins and patches of altered rock were removed before the sample was ground and sieved to prepare the gouge.

[8] The chrysotile gouge was prepared from an essentially pure clinochrysotile sample from New Idria, California. Of the three serpentinite minerals tested, the chrysotile is closest to end-member composition, with only about 0.35 wt% Al_2O_3 and ~0.2 wt% FeO.

Table 1. Summary of Experiments (All Conducted at 100 MPa Effective Normal Stress)

Gouge	Driving Blocks	T (°C)	Axial Displacement Rate(s) ($\mu\text{m/s}$) ^a	Jacket	Examination of Run Products
Antigorite	Granite	200	0.01	Ag	ThS
Antigorite	Granite	250	0.01	Cu	SEM, XRD
Antigorite	Granite	300	0.01	Cu	ThS, SEM
Antigorite	Granite	350	0.01	Ag	ThS, SEM
Antigorite	Quartzite	250	0.1	Cu	ThS
Antigorite	Quartzite	250	0.01	Cu	SEM, XRD
Antigorite	Quartzite	250	0.01–0.1	Cu	ThS
Antigorite	Quartzite	250	0.001–0.01	Cu	ThS, SEM
Antigorite	Serpentinite	250	0.01	Cu	ThS, SEM, XRD
Antigorite	Serpentinite	250	0.001–0.1	Cu	
Lizardite	Granite	250	0.01	Cu	XRD
Lizardite	Granite	250	0.001–0.01	Ag	SEM, XRD
Lizardite	Granite	200	0.0032–0.01	Cu	ThS
Lizardite	Granite	200	0.001–0.32	Pb	
Lizardite	Quartzite	200	0.01	Pb	
Lizardite	Quartzite	250	0.01	Cu	SEM, XRD
Lizardite	Quartzite	250	0.001–0.01	Ag	SEM, XRD
Lizardite	Serpentinite	250	0.01	Cu	ThS, SEM
Lizardite	Serpentinite	250	0.001–0.1	Cu	
Chrysotile	Granite	250	0.01	Cu	XRD
Chrysotile	Serpentinite	250	0.01	Cu	
Granite	Granite	250	0.01	Ag	ThS
Quartz	Quartzite	250	0.01	Ag	ThS

^aShearing rates within inclined gouge layer are 15.5% higher. ThS, thin section; SEM, scanning electron microscope; XRD, powder X-ray diffraction.

2.1.2. Quartz-Rich Starting Materials

[9] The Westerly granite stock contains about 44% by volume plagioclase, with oligoclase (An_{17}) cores and albite (An_9) rims, ~28% quartz, 21% K-feldspar (Ab_7), and 6% biotite. Accessory minerals include muscovite, chlorite, epidote, and titanite. A more detailed rock description, along with mineral compositions determined by electron microprobe techniques, is contained in *Moore et al.* [1987]. As with the serpentinite gouges, the granite was crushed and sieved to $<90\ \mu\text{m}$ grain size to produce a synthetic gouge.

[10] The quartzite used for the driving blocks is nearly pure quartz, with trace amounts of white K-mica that fills some interstices [*Moore et al.*, 1987]. The quartz gouge is from the same stock used by *Tembe et al.* [2010] and *Moore and Lockner* [2011] for friction experiments on mixtures of quartz with a variety of phyllosilicate minerals. It is a commercially acquired Ottawa sand ($>99\%$ quartz) that had been crushed and sieved by *Tembe et al.* [2010] to $<180\ \mu\text{m}$ grain size.

2.2. Experimental Procedures

[11] The experiments (Table 1) were run in a triaxial deformation apparatus, using the furnace assembly shown in Figure 1a. Each sample consisted of a rock cylinder

41 mm in length and 19.1 mm in diameter that was sliced into two pieces at a 30° angle to the cylinder axis. The sawcut surfaces were hand lapped with 120-grit SiC to provide a uniform surface roughness. A thin layer of the gouge to be tested was smeared as a stiff paste onto the lower driving block to an initial thickness of 1 mm (compacting to 0.6–0.7 mm during an experiment), and the upper block was then placed on top of the gouge layer. The upper driving block contained a throughgoing, 2.5 mm diameter borehole to ensure good communication between the external pore-pressure system and the fluids within the gouge layer. A hollow steel tube (2.35 mm outer diameter, 0.8 mm opening at the base and 1.5 mm opening at the top) was inserted into the borehole, to minimize extrusion of gouge into the opening. The assembled sample was placed in a jacket between titanium carbide end plugs and alumina insulators. The space between the jacketed assembly and the furnace was loosely packed with powdered boron nitride, a good thermal and poor electrical conductor, which was held in place with the aid of fiberglass cloth tape. During an experiment, a steel piston advanced against the base of the sample column (Figure 1a), resulting in shear within the gouge layer (Figure 1b).

[12] All experiments were conducted at a pore-fluid pressure of 50 MPa and constant normal stress of 150 MPa, for an effective normal stress of 100 MPa. Temperatures ranged between 200 and 350°C , representing the deeper part of the seismogenic zone of continental crust. With one exception, axial displacement rates varied between 0.001 and $0.1\ \mu\text{m/s}$ (Table 1), corresponding to shearing rates along the sawcut of about 3.6–360 cm/yr. Once in the pressure vessel, confining pressure (argon gas) was first raised to ~70 MPa while the pore-pressure lines were being evacuated. The evacuation process lasted about 20 min; immediately after that, a 50 MPa fluid pressure was applied. Confining pressure rose to the starting value of 150 MPa as the sample was heated. Setup time for the experiment following heating was typically ≥ 30 min. Temperature was monitored at the top of the sample by a thermocouple inserted along the pore-pressure inlet (Figure 1a). Constant normal stress was maintained during the experiments by means of computer-controlled adjustments to confining pressure.

[13] The absolute value of seal friction was subtracted from the load-cell reading before sample contact. Because seal friction is a function of confining pressure, an additional correction was applied during the experiment to account for the continuing adjustments to the confining pressure. Corrections for changes in contact area along the sliding surface were made during the experiment as described by *Scott et al.* [1994] and *Tembe et al.* [2010]. A greased Teflon shim was placed between the sample and forcing piston (Figure 1a) to allow lateral slip of the lower driving block during shear. The correction to the normal stress for lateral slip on the Teflon shim is +0.7 MPa. Because the coefficient of friction is the ratio of shear stress to effective normal stress, systematic errors due to seal friction, stress calibrations, and sample contact area partially cancel in computing the ratio.

[14] The shear resistance of the jacket was removed from the total shear stress after the experiment. Three different jacketing materials with different strength profiles—Cu, Ag, and Pb—were used in this study (Table 1). Jacket wall thicknesses were 0.38 mm for Cu and Ag, and 0.50 mm

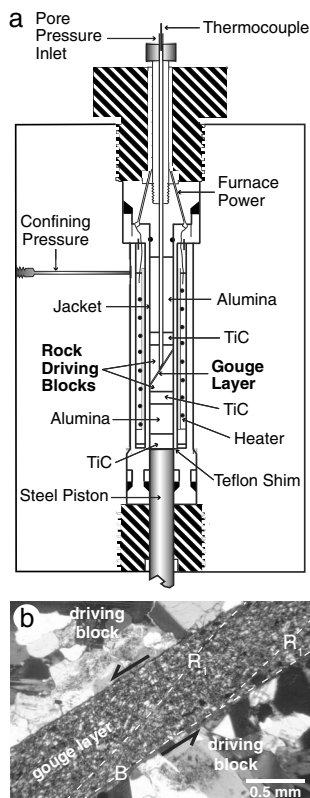


Figure 1. (a) Experimental assembly (TiC, titanium carbide). (b) Photomicrograph (crossed polarizers) of antigorite gouge sheared between granite driving blocks. In all experiments, shear in the gouge layer, whatever its mineral content, was highly localized along subsidiary shears (highlighted by dashed lines) that form close to the gouge-rock boundary (boundary shears, B) and that cross the gouge layer at relatively small angles (low-angle Riedel shears, R_1).

for Pb. Corrections for the Pb and annealed Cu jackets are reported in *Moore and Lockner* [2011]. A stock of annealed silver jackets was prepared and tested during this study and used for some of the final experiments, including the two longest-duration ones (~11 and ~15 days). The total correction to the shear strength at elevated temperatures is ~1–2 MPa lower for Ag than for Cu. We estimate that typical uncertainties in determining coefficient of friction are ± 0.02 for Pb jacket tests and ± 0.03 for experiments run in Cu or Ag jackets.

3. Results of Experiments

[15] The experiments conducted for this study can be separated into two groups. The first set (Figures 2–4) highlights the influence of wall-rock composition on the strengths of different gouge materials, all tested at 250°C and 0.01 $\mu\text{m/s}$ axial displacement rate (0.0115 $\mu\text{m/s}$ shearing rate on the sawcut surface). The second group (Figures 5–7) considers the effects of temperature and shearing rate on the strengths of serpentinite gouges sheared between quartz-bearing rocks.

3.1. Effect of Wall Rocks on Strength

[16] The results of the control experiments (Figure 2) are all consistent with previously published friction data on these materials. The quartz and granite gouges have nearly identical strength-displacement behavior, with coefficients of friction, μ , in excess of 0.7. *Chester and Higgs* [1992] also reported $\mu \sim 0.7$ between 25 and 300°C for water-saturated quartz gouge at 150 MPa effective confining pressure. Westerly granite sheared between granite blocks by *Blanpied et al.* [1995] approached $\mu \sim 0.8$ after 4 mm axial

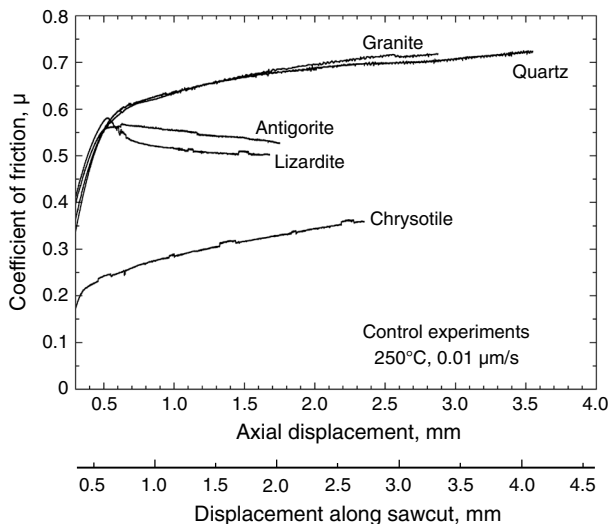


Figure 2. Control experiments at 250°C and 0.01 $\mu\text{m/s}$ axial displacement rate (0.0115 $\mu\text{m/s}$ along the sawcut). Serpentinite gouges were sheared between driving blocks of serpentinite in Cu jackets, quartz gouge between quartzite blocks (Ag jacket), and granite gouge between blocks of Westerly granite (Ag jacket). Periodic steps in the chrysotile and lizardite data are caused by an unresolved electronic problem that occurs twice daily, at the same times each day.

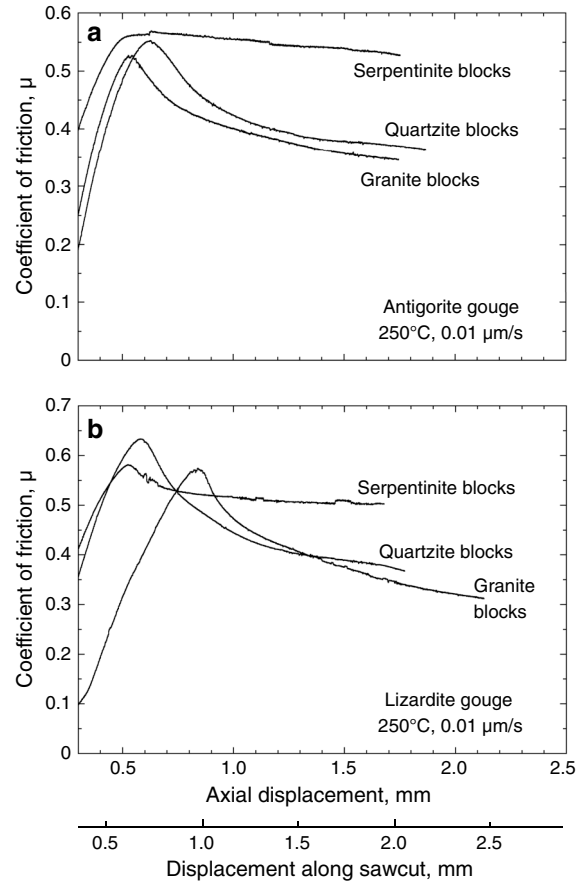


Figure 3. Effect of “wall rocks” on shear of (a) antigorite and (b) lizardite gouges at 250°C and 0.01 $\mu\text{m/s}$ axial displacement rate. The experiments using serpentinite driving blocks are from Figure 2; all experiments used Cu jackets.

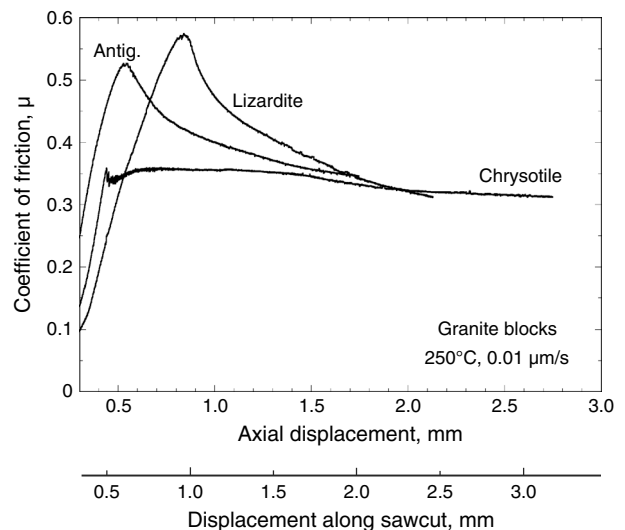


Figure 4. Frictional strengths of the three serpentinite gouges sheared between granite blocks in Cu jackets at 250°C and 0.01 $\mu\text{m/s}$ axial displacement rate. At axial displacements greater than 1.5 mm, strengths of the three serpentinite gouges are closely comparable.

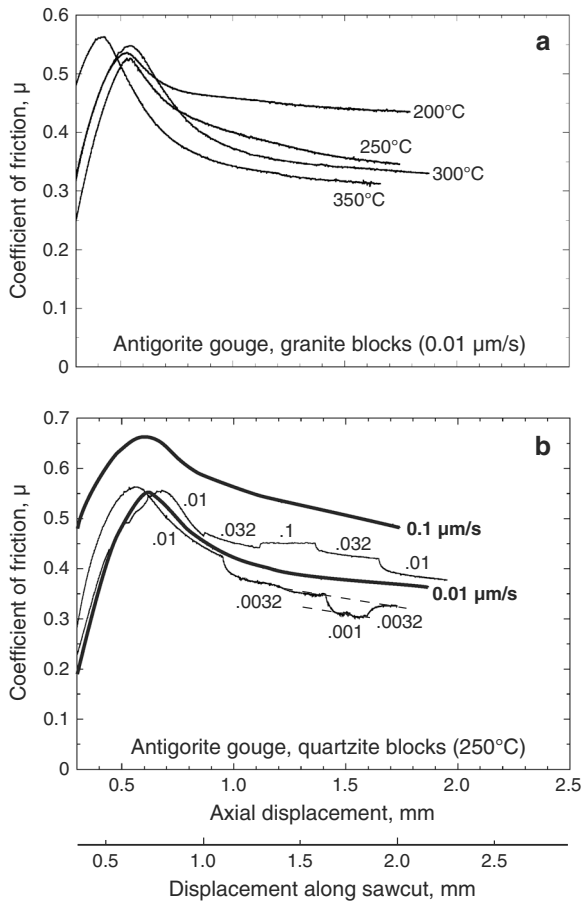


Figure 5. Effects of (a) temperature and (b) sliding velocity on the strength of the antigorite gouge. Experiments in Figure 5a used granite driving blocks and were run at $0.01 \mu\text{m/s}$ axial displacement rate. Experiments at 250°C and 300°C were run in Cu jackets and those at 200°C and 350°C in Ag jackets. Final gouge-layer thickness did not vary with temperature. Experiments in Figure 5b used quartzite blocks and Cu jackets and were run at 250°C .

displacement at 250°C and 400 MPa effective normal stress. The serpentinite gouges are all weaker than the quartz-bearing ones, with $\mu = 0.50\text{--}0.55$ for lizardite and antigorite. Chrysotile has somewhat lower strength than the other two serpentinite gouges, but μ exceeded 0.35 and the sample was continuing to strain harden when the jacket failed. The serpentinite data are consistent with our previously reported results for these same gouges tested at similar temperatures [Moore et al., 1997, 2004; Moore and Lockner, 2007].

[17] As illustrated in Figure 3, wall-rock chemistry has a marked effect on the strengths of the antigorite and lizardite gouges, measured in otherwise identical experiments lasting 2–2.5 days. The initial strength-displacement trends in each figure are similar up to the peak strength, where $\mu > 0.5$. Beyond the peak, however, both gouges weakened continuously when sheared between quartz-rich rocks, such that $\mu < 0.4$ at the time that the jackets failed. The strengths of the two serpentinites had not leveled off by the end of the experiments, although the rates of decrease of μ had slowed substantially. Strengths were slightly lower with granite than with quartzite blocks.

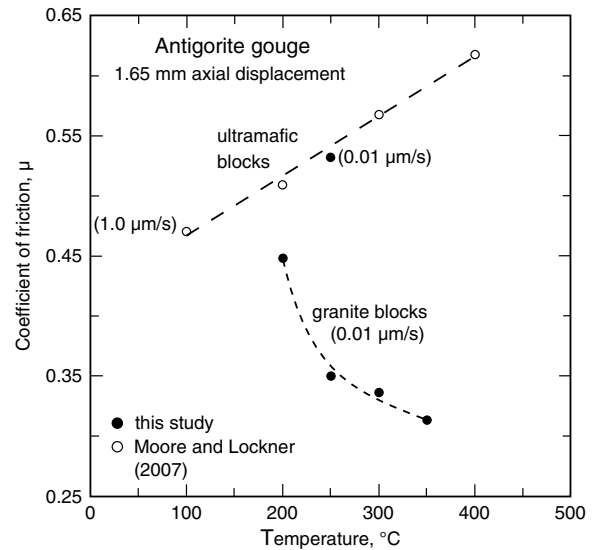


Figure 6. Temperature and compositional controls on antigorite frictional strength. Reported values of μ were measured at 1.65 mm axial displacement (1.90 mm shear displacement), which is the maximum axial displacement attained by all of the samples. Data for antigorite sheared between ultramafic rocks at $1.0 \mu\text{m/s}$ are from Moore and Lockner [2007].

[18] Chrysotile, which is weaker than antigorite and lizardite at 250°C (Figure 2), is not substantially weakened by the substitution of granite for serpentinite driving blocks (Figure 4). Notably, however, the strengths of all three serpentinite gouges essentially converge at axial displacements greater than ~ 1.5 mm. The remaining experiments focused on the antigorite and lizardite gouges, because of their more substantial response to the presence of quartz-rich rocks.

3.2. Effects of Temperature and Sliding Rate on Strength

[19] In a granitic environment, the antigorite gouge weakens by $\sim 25\%$ between 200 and 350°C , with the largest decrease in the interval 200– 250°C (Figure 5a). The temperature effect is highlighted in Figure 6, which compares the strengths measured at 1.65 mm axial displacement (the maximum displacement reached by all four samples) for the experiments in Figure 5a with our earlier results for antigorite gouge [Moore and Lockner, 2007]. When the antigorite gouge is sheared between the ultramafic rocks, the μ increases by about 30%, from ~ 0.47 to ~ 0.62 , with increasing temperature in the range 100– 400°C . Although the data from Moore and Lockner [2007] were measured at a higher velocity of $1.0 \mu\text{m/s}$, the control experiment run at $0.01 \mu\text{m/s}$ (Figure 2) fits the trend for those experiments. At 350°C , substituting granite for ultramafic driving blocks lowers μ by ~ 0.25 (Figure 6), a roughly 40% reduction.

[20] The antigorite gouge is also characterized by a marked rate dependence of μ in experiments using the quartzite driving blocks (Figure 5b). Considering first the two runs at a single velocity, the one at $0.01 \mu\text{m/s}$ is shifted below the one at $0.1 \mu\text{m/s}$ by approximately $\mu = 0.1$. The differences in strength measured during the two velocity-stepping experiments are most pronounced at the slowest

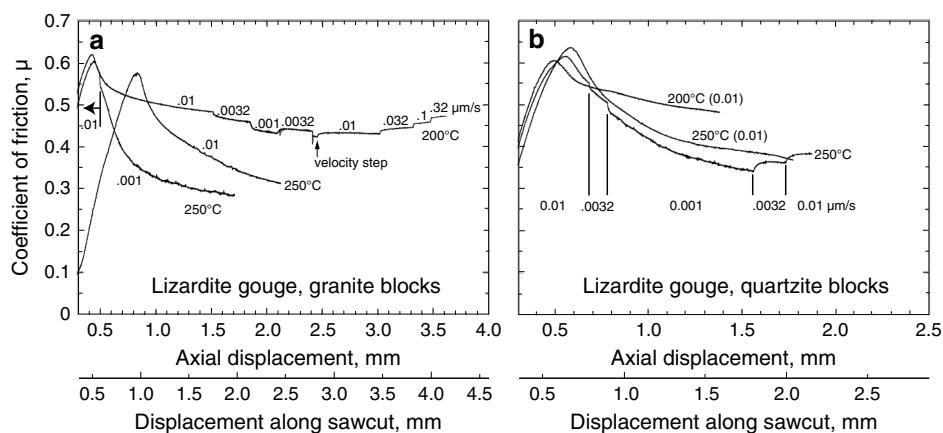


Figure 7. Effects of sliding velocity and temperature on lizardite gouge sheared between (a) granite and (b) quartzite blocks. Jacketing materials were 200°C, Pb; 250°C and 0.01 $\mu\text{m/s}$, Cu; and 250°C and 0.001–0.01 $\mu\text{m/s}$, Ag.

velocities. For the experiment run between 0.01 and 0.1 $\mu\text{m/s}$, the first two velocity steps are somewhat smaller than the reversed steps made later in the experiment. The effect of changes in sliding velocity on μ is considered in more detail in the next section.

[21] Experiments on the lizardite-rich gouge (Figure 7) yielded results similar to those for antigorite. The substantial decrease in strength with increasing temperature from 200 to 250°C mirrors that found for antigorite (Figure 5a). In all cases, strength increases with increasing velocity. The changes in μ accompanying the first two velocity steps in the 250°C experiment in Figure 7b appear smaller than the same steps made in reverse order at the end, as was also observed during an antigorite experiment (Figure 5b).

3.3. Velocity Dependence of Strength

[22] The effect of a change in shearing velocity typically is calculated as $\Delta\mu_{ss}/\Delta\ln V$, where $\Delta\mu_{ss}$ is the change in steady state coefficient of friction, which follows a logarithmic change in velocity, V . Estimates of $\Delta\mu_{ss}/\Delta\ln V$ obtained from the velocity-stepping experiments in Figures 5 and 7 are plotted in Figure 8; the calculation procedures are summarized in Appendix A. Few published velocity data at elevated temperatures from all-serpentinite experiments are available for comparison. To remedy this, data for the lizardite gouge at $\sim 200^\circ\text{C}$ from Moore *et al.* [1997] were augmented by new experiments at 250°C on the lizardite and antigorite gouges (Figure A1 in Appendix A).

[23] In previous studies using serpentinite blocks, the serpentine minerals showed both positive and negative values of $\Delta\mu_{ss}/\Delta\ln V$ that varied irregularly with changing temperature, pressure, and velocity [Reinen *et al.*, 1991, 1994; Moore *et al.*, 1997]. Of the data set in Figure 8, only the lizardite gouge tested at 200°C yielded negative values (Figure 8a), although some of the 250°C data obtained from both gouges are at or near 0 (Figures 8b and 8c). The lizardite and antigorite gouges have opposite trends in $\Delta\mu_{ss}/\Delta\ln V$ with increasing velocity at 250°C.

[24] A systematic investigation of the rate dependence of strength was not done in this study. Nevertheless, only velocity-strengthening behavior was observed during shear of serpentinite against quartz-rich rocks (Figure 8). The

velocity steps made just after peak strength during two experiments, which appeared to be relatively small as described previously, are similar to the data from the serpentinite-block experiments (Figures 8b and 8c). The same velocity steps made later in those two experiments have substantially larger values. Overall, $\Delta\mu_{ss}/\Delta\ln V$ increases with decreasing velocity in each serpentinite gouge-quartzose rock experiment. The most marked response to the change in driving blocks was shown by the antigorite gouge at 250°C; at the slowest velocity step, substituting quartzite for serpentinite driving blocks increased $\Delta\mu_{ss}/\Delta\ln V$ by ~ 0.025 (Figure 8c).

4. Microtextural Observations

4.1. Methods

[25] Ten of the tested samples were examined with a scanning electron microscope (SEM) equipped with an energy dispersive X-ray fluorescence system (EDS) (Table 1), to look for textural and mineralogical evidence of the processes that occurred during the experiments. First the jackets were removed from these samples and the driving blocks separated, to permit preliminary study of the gouge layers with a stereomicroscope. Selected oriented fragments of gouge were then mounted on plugs for the SEM work. The remaining gouge from six of these experiments was ground for powder XRD analysis (Table 1).

[26] Covered thin sections were prepared from 11 samples for examination with a petrographic microscope. To prepare the thin sections, the jacketed samples were epoxied before being sliced parallel to the length of the cylinder and perpendicular to the sawcut. Some of the half cylinders remaining from the thin-sectioning process were subsequently mounted onto glass slides for SEM viewing. Although the slicing renders the surface unsuitable for microtextural analysis, the major structural features are preserved. In addition, the half cylinders proved very useful for the examination of pore spaces in the gouge immediately below its surface.

4.2. Observations

[27] Our previous petrographic studies of water-saturated serpentinite gouges sheared between ultramafic rocks at

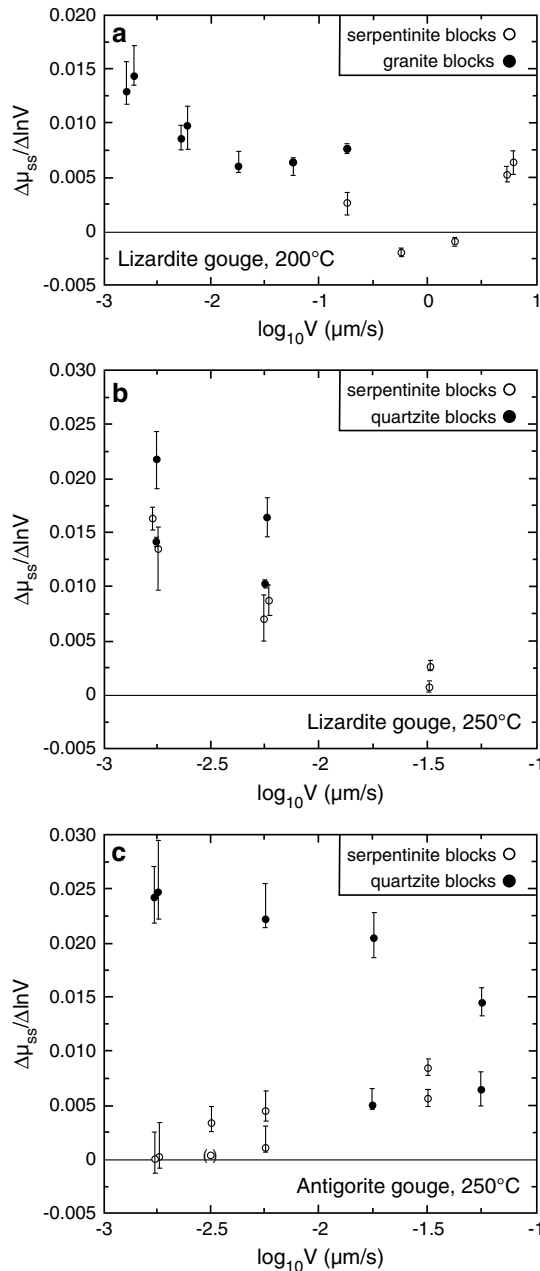


Figure 8. Steady state velocity dependence of frictional strength. (a) Velocity data for lizardite gouge tested at 200°C, from Figure 7a and Moore *et al.* [1997]. (b) Data for lizardite gouge at 250°C, from Figures 7 and A1a. (c) Data from the antigorite gouge experiments in Figures 5b and A1b. The horizontal axis is the log of axial velocity, and each value of $\Delta\mu_{ss}/\Delta\ln V$ is plotted at the midpoint of the velocity step.

temperatures up to 400°C yielded no evidence of recrystallization of the serpentine minerals; rather, brittle deformation features dominated [e.g., Moore *et al.*, 1997, Figure 8; Moore and Lockner, 2007, Figure 6]. In those experiments, deformation was concentrated along the shear planes and included grain-size reduction and rotation of anisotropic mineral grains into parallelism along boundary (B) and low-angle Riedel (R_1) shears [e.g., Moore *et al.*, 2004,

Figure 5]. Overall, the gouge between the shears was compacted but not substantially deformed, and considerable porosity remained. The main exceptions occurred near the intersections of R_1 and B shears, where the gouge sandwiched between the shears was relatively highly compacted and somewhat foliated.

[28] These same brittle deformation features were also major elements of the serpentinite gouge samples sheared between granite and quartzite blocks. Viewed in thin section (Figure 1b) or under a stereomicroscope, no obvious textural differences from the ultramafic-block experimental samples could be discerned. However, SEM examination did reveal some differences. The serpentinite gouges from shorter-duration runs (≤ 6 days) between quartz-bearing rocks showed evidence of the neocrystallization of serpentine minerals. In a lizardite sample sheared between quartzite blocks at 250°C for ~ 2 days (Figures 9a–9c), numerous tiny hexagonal platelets with EDS spectra characteristic of serpentine (Figure 9a) are present in the narrow band of gouge between a B and an R_1 shear. The platy shape is suggestive of the crystallization of lizardite. Euhedral crystals such as these were not seen in gouge layers from purely ultramafic experiments. Additional hexagonal platelets of serpentine, as indicated by EDS, were found above a partly exposed B shear (Figure 9b), and a few narrow fibers (chrysotile?) were seen in the gouge between another R_1 and B shear (Figure 9c).

[29] A second example (Figures 9d and 9e) is from an experiment in which antigorite gouge was sheared between quartzite blocks for ~ 6 days at 250°C. Both hexagonal platelets and stubby tubes, ~ 300 – 400 nm in maximum dimension, crystallized on serpentine grains in the gouge between R_1 and B shears (Figure 9d). Nearby, clusters of tubular serpentine, as indicated by EDS analysis, extend 2–3 μm into a pore space from the surface of a gouge grain (Figure 9e).

[30] The longest experiment, which lasted ~ 15 days, consisted of lizardite gouge sheared between granite blocks at 250°C, largely at 0.001 $\mu\text{m/s}$ (Figure 7a). In contrast to the shorter experiments, this sample showed clear evidence of the crystallization of Mg-rich smectite clays in both the serpentinite gouge and the adjacent wall rocks (Figure 10), whereas no new growth of serpentine was observed. Portions of the B shears are covered with smectite clays that display the characteristic curled edges (Figure 10a) caused by dehydration in the vacuum system of the SEM [e.g., Welton, 1984]. The clay-bearing B shear surface has a wavy texture, and in places, a few pores are present (Figure 10b). EDS spectra of these minerals are consistent with the Mg-rich smectite clay, saponite (Figure 10c). Saponite is a trioctahedral smectite clay whose crystal structure is derived from that of talc by substitution of Al for Si in the tetrahedral sheet (ideally 0.33 atoms per 4 Si). The resulting negative layer charge is balanced by the addition of interlayer cations, in this case principally Na and K (Figure 10c). The Mg-rich clays are concentrated on the B shears in the gouge layers. Although some clays are also found on R_1 shears, their occurrence is restricted to those portions located closest to the B shears. The remainder of the gouge layer appears to lack clays. The total volume of smectite in the gouge layer is small; no peaks attributable to a smectite mineral were seen in a powder XRD pattern of the bulk gouge.

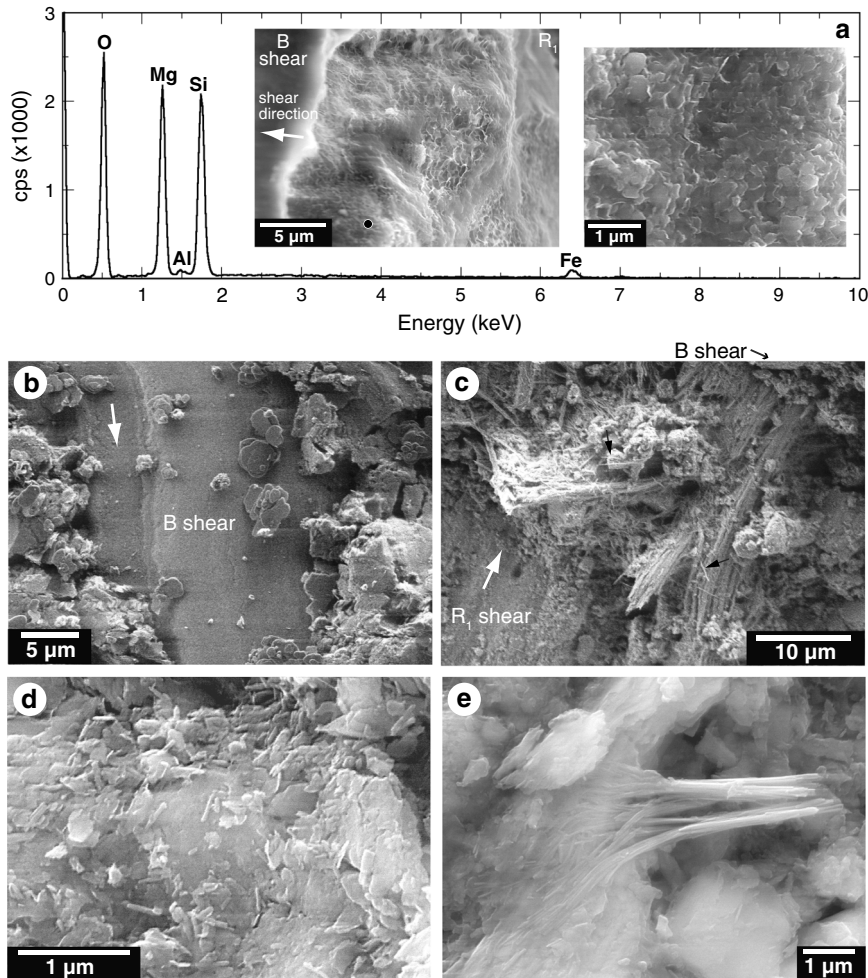


Figure 9. Crystallization of serpentine minerals during some experiments. All of the photos are secondary-electron SEM images. White arrows indicate the direction of movement of the shear planes in the images. (a–c) Lizardite gouge sheared between quartzite blocks, 250°C, ~2 day experiment. (a) Energy-dispersive system X-ray fluorescence (EDS) spectrum of serpentine platelets in the area between a B and R₁ shear. The analyzed spot is marked by the filled circle in the inset photo at left. The inset photo at right is a higher magnification view of a portion of the same surface. (b) Euhedral hexagonal platelets of serpentine (lizardite?) on a B shear. These loose crystals and the gouge atop the shear plane are portions of the thin layer of gouge located between the shear and the sawcut surface of the driving block. (c) Thin fibers (indicated by black arrows) of possible chrysotile deposited in random orientations in gouge between a B and R₁ shear. (d–e) Antigorite gouge sheared between quartzite blocks at 250°C, ~6 days duration. Secondary-electron SEM images are taken near the intersection of a B and R₁ shear. (d) Stubby tubes and thin hexagonal platelets of serpentine averaging ~300–400 nm in longest dimension on grains in serpentinite gouge. (e) Cluster of serpentine tubes (determined by EDS) growing into open void space of the gouge. Numerous shorter tubes and hexagonal plates dot the surface of the gouge grain near the base of the projecting crystals.

[31] The granite exposed on the sawcut surface also shows evidence of mineral dissolution and crystallization. Microcracks in the quartz and K-feldspar crystals in Figures 10d and 10e, respectively, have been significantly widened by dissolution, and the surface of the K-feldspar crystal is heavily pitted. Numerous Mg-rich smectite clays have crystallized on the igneous minerals, and their chemical composition is the same as that of the clays in the gouge layer.

[32] The other long-duration experiment (~11 days) was conducted on lizardite gouge sheared between quartzite

blocks at 250°C (Figure 7b). Some quartz crystals at the sawcut surface appear slightly etched. Several euhedral, platy serpentine crystals were identified at or near the shear surfaces in the gouge, along with a few crystals of other Mg-rich phyllosilicate minerals. The textures and relative proportions of Si, O, and Mg of some grains are consistent with a smectite clay, possibly stevensite, whose chemistry (relatively low Al, no Na or K) differs from that of the clays from the granite driving-block experiments. The composition of some other crystals is more consistent with talc. The replacement of serpentine + quartz by talc has been described

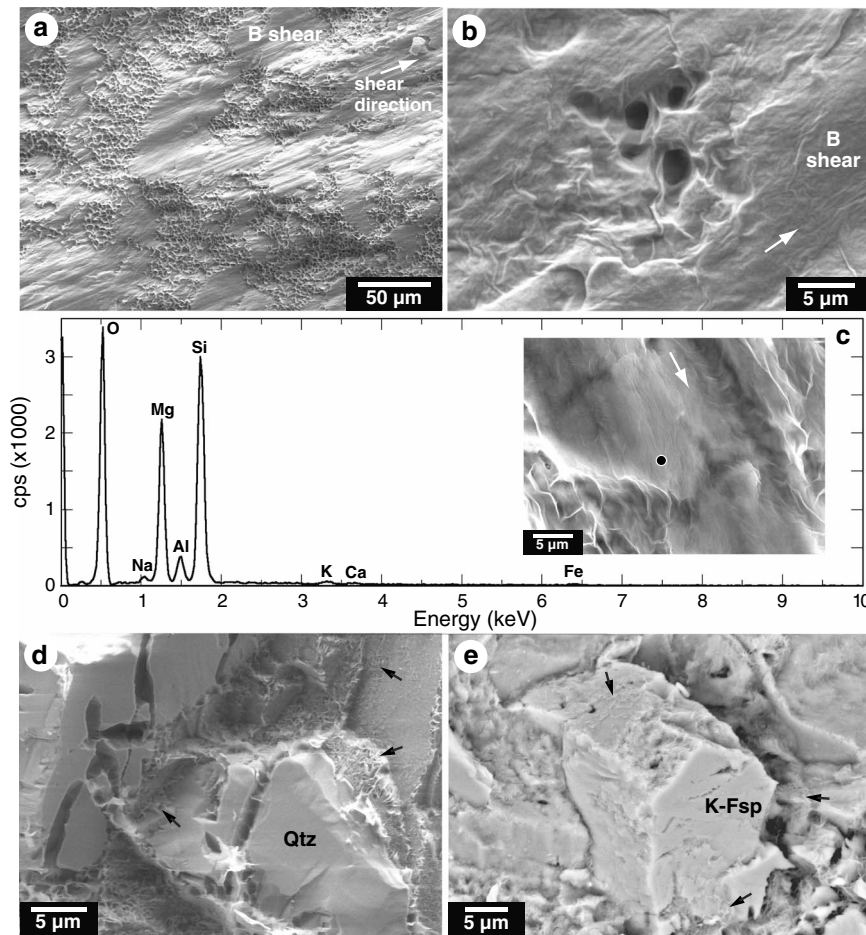


Figure 10. Growth of Mg-rich smectite clays during a 15 day experiment at 250°C in which lizardite was sheared between granite blocks. White arrows indicate the direction of motion of the exposed B shear surface. (a) B shear covered with smectite clays, whose curled edges result from drying under evacuation. (b) Closer view of smectite clays and a small cluster of pores on a B shear surface. (c) EDS spectrum of the Mg-rich, likely saponitic smectite clay, with interlayer cations Na and K. The filled circle on the inset photo is the location of the analyzed spot on the B shear. (d) Quartz (Qtz) crystal on the granite sawcut surface has an etched appearance from dissolution concentrated along cracks. Deposits of Mg-rich smectite clays (black arrows) cover part of the surface. (e) K-feldspar (K-Fsp) crystal from the granite adjoining the gouge has a pockmarked appearance caused by dissolution, and it is partly covered with Mg-rich smectite clays (black arrows).

in recent hydrothermal experiments conducted at 350°C [Ellis *et al.*, 2010] and shearing tests in the presence of a pore fluid at 300–500°C [Hirauchi *et al.*, 2013].

5. Discussion

5.1. Weakening Mechanisms of Serpentinite Faulted Against Quartzofeldspathic Rocks

[33] Our experiments demonstrate that antigorite- and lizardite-rich serpentinite gouges are dramatically weakened (by as much as 40%) at hydrothermal conditions ($T \geq 200^\circ\text{C}$), when sheared against quartz-bearing rocks compared to ultramafic rocks. Measurable weakening occurred within ~ 2 days at 200°C, the lowest temperature tested in this study, suggesting that the weakening mechanism may be effective at even lower temperatures over longer time intervals. In a quartzofeldspathic environment, serpentinite gouge strength decreases markedly with increasing temperature, the

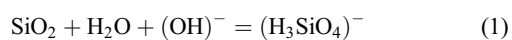
opposite of its behavior in an ultramafic system. In addition, only velocity-strengthening behavior was observed, and the measured values of $\Delta\mu_{ss}/\Delta\ln V$ are highest at the highest temperature and slowest velocity tested. The frictional strengths of antigorite, lizardite, and chrysotile gouges all reach similar values during shear between granite blocks (Figure 4). Magnesium-rich phyllosilicates crystallized during the experiments, the identity of the minerals changing with time and with wall-rock chemistry. The critical role of a fluid phase is illustrated by tests on oven-dried samples that yielded $\mu \sim 0.75$ for antigorite serpentinite independent of wall-rock chemistry at 250–300°C [Moore and Lockner, 2007; Moore *et al.*, 2010].

[34] The operation of a fluid-activated, temperature- and rate-dependent weakening mechanism in the serpentinite in these experiments is consistent with a solution-transfer creep process [e.g., Rutter and Mainprice, 1978, 1979; Chester and Higgs, 1992; Chester, 1995; Blanpied *et al.*, 1995; Bos and

Spiers, 2001]. The process involves mineral dissolution at one site, followed by diffusion of the dissolved material to a new location where mineral precipitation occurs. Both cataclastic (i.e., grain sliding, rolling, and crushing) and solution-transfer processes are operative to varying degrees in rocks throughout the upper crust. The hydrothermal experiments and modeling of *Chester and Higgs* [1992] and *Chester* [1995] on quartz and *Blanpied et al.* [1995] on granite indicate that cataclasis is the dominant deformation mechanism in quartzose crustal rocks at temperatures below 300–350°C, whereas both solution-precipitation creep and cataclasis are important at higher temperatures (mid-crustal depths). This transition in frictional behavior marks the base of the seismogenic zone in continental crust. The effect of the quartz-bearing wall rocks on the frictional behavior of serpentinite is such that the aseismic slip and weakening become important at *T-P* conditions that normally would correspond to depths within the seismogenic zone.

[35] We propose that modifications to the chemistry of the pore fluids resulting from interaction with the granite and quartzite wall rocks significantly enhance the solubility and/or the rate of dissolution of serpentine compared to a purely ultramafic chemical system, thereby promoting the solution-transfer process. Because of the lack of information about fluid chemistry in our samples, we use the chemistry of natural groundwaters to speculate on possible causes. *Barnes et al.* [1972] analyzed the waters issuing from surface springs associated with ultramafic bodies in California and found that water chemistry varied with the direction of flow of the fluids relative to the ultramafic rock. Fluids sampled from the interiors of large ultramafic bodies are “ultrabasic waters” (pH = 11.8–12.1) whose thermodynamic properties are entirely controlled by reaction with the ultramafic host rocks, even though their isotopic signatures indicate diverse origins from meteoric or connate sources. These waters also have low dissolved silica contents (<25 mg/L SiO₂), and they are highly undersaturated with respect to quartz [see also *Barnes and O’Neil*, 1969]. Groundwaters issuing from springs sited along the contacts between antigorite serpentinite and metadacite bodies are somewhat less basic, with pH = 10.8–10.9, and they are supersaturated with respect to quartz, having dissolved silica contents as high as 4000 mg/L SiO₂. *Barnes et al.* [1972] concluded that these fluids must have flowed along the contact and interacted with the rocks on both sides.

[36] Dissolution experiments conducted on lizardite [*Luce et al.*, 1972], antigorite [*Lin and Clemency*, 1981], and chrysotile [*Bales and Morgan*, 1985] all demonstrate that both the solubility and rate of dissolution of serpentine, and especially the rate of release of Mg to solution, increase with decreasing pH. *Bales and Morgan* [1985] suggested that dissolution at higher-energy surface sites, in particular, may be pH dependent. The two groups of groundwaters analyzed by *Barnes et al.* [1972] differ by only 1 pH unit; nevertheless, the lower pH of the waters in contact with both metadacite and serpentinite will favor at least some increase in serpentine solubility, even if it is not the sole factor. Dissolution of quartz combined with ionization of dissolved silica species in basic pore fluids [*Krauskopf*, 1967]



will maintain pH at a lower value than in a quartz-absent chemical system.

[37] The modifications to fluid chemistry that markedly enhance dissolution of the serpentine minerals are just one aspect of the chemical processes operative during the experiments, whose effects also include changes in the Mg-rich minerals that precipitate over time. Serpentine minerals crystallized during experiments of ≤6 days duration. The two longest experiments (>10 days) showed incipient crystallization of new Mg-rich phyllosilicates, whose compositions varied with the mineralogy of the wall rocks.

[38] The reaction zones characteristically developed at the contacts between ultramafic and crustal rocks have long been studied as classic examples of metasomatism [e.g., *Jahns*, 1967; *Sanford*, 1982; *Coleman*, 1967; *Mori et al.*, 2007]. Mass transfer across the contact is driven by chemical potential gradients between the rocks on either side. *Frantz and Mao* [1976, 1979] modeled the development of ultramafic reaction zones as a metasomatic solution-transfer process. Material transfer occurs via intergranular water films by one or both of two mechanisms: (1) diffusion through a stationary pore fluid and (2) convective transport (infiltration) due to motion of the pore fluid relative to the solid framework. A progressive mineral zonation develops on either side of the contact, as illustrated in the experimental investigation conducted by *Koons* [1981]. He placed antigorite serpentinite next to a quartzofeldspathic rock in gold tubes, filled them with water and sealed them, and then held them at 450°C and 200 MPa confining pressure for periods of 15–40 days. New minerals, including talc, tremolite, and chlorite, formed in specific zones at the ultramafic-schist contact, mimicking natural occurrences. He identified different stages of reaction over time—an initial stage of volatile metasomatism (e.g., CO₂), followed by migration of SiO₂ and subsequently other non-volatile elements. The studied natural reaction zones typically are on the scale of meters, and many meter-scale pods of one rock type embedded in the other have lost all traces of the original mineral assemblage [e.g., *Coleman*, 1961; *Sanford*, 1982].

[39] The textural and mineralogical changes that occurred over time in the shearing experiments are readily explained in terms of such diffusive mass-transfer processes. Reprecipitation of serpentine minerals in the gouge dominated in the short-term experiments, whereas different Mg-rich phyllosilicates crystallized during the 11 day quartzite experiment (talc + smectite (stevensite?)) and the 15 day granite experiment (saponite). Saponitic clays of similar chemistry grew in the serpentinite gouge and on the surface of the granite wall rocks, indicating migration of Si, Al, Na, and K (provided by dissolution of quartz and feldspars; Figures 10d and 10e) into the gouge and of Mg (released by dissolution of serpentine) toward the wall rocks. It should be noted that the smectite clays in the 250°C experiments are likely metastable minerals that crystallized at temperatures above their normal thermal stability range due to favorable growth kinetics. Observed mineralogical changes in the gouge layers were limited to shears located close to the contact with the driving blocks, putting the scale of diffusion at tens of micrometers for those experiments.

[40] The Mg-smectite clay saponite is extremely weak, $\mu \sim 0.05$ at room temperature and 100 MPa effective normal stress [*Lockner et al.*, 2011]. Talc is similarly weak

at temperatures in the approximate range 200–300°C [Moore and Lockner, 2008]. The presence of small amounts of these neocrystallized minerals did not noticeably affect strength during the two long experiments run largely at 0.001 $\mu\text{m/s}$ (Figure 7). Eventually, however, sufficient amounts of these weak minerals would crystallize such that they would influence the frictional behavior of the gouge during an experiment.

5.2. Application to Fault Zones

5.2.1. Faults Juxtaposing Serpentine and Crustal Rocks

[41] Our results show that, in the absence of geometric or other impediments, any active crustal fault that shears serpentinite against quartzofeldspathic rocks has the potential for aseismic slip (creep) at seismogenic depths. In particular, these results offer a possible explanation for the long-noted geographic association of serpentinite with creeping faults of the San Andreas system in central and northern California [e.g., Allen, 1968; Hanna *et al.*, 1972; Irwin and Barnes, 1975; Irwin, 1990; Titus *et al.*, 2011]. This inferred correlation of serpentinite with fault creep needs to be tested in considerably more detail to assess its validity. As a result of long-term monitoring efforts [e.g., Galehouse and Lienkaemper, 2003; McFarland *et al.*, 2009], the occurrence and rates of creep have been documented along several faults in the San Francisco Bay area. Detailed field mapping and geophysical investigations are now needed to determine whether or not the occurrence and distribution of serpentinite at depth can be correlated to the patterns of creep along those faults.

[42] Core recovered as part of the San Andreas Fault Observatory at Depth (SAFOD) deep drilling program [e.g., Zoback *et al.*, 2011] does link serpentinite with creep along the central San Andreas fault. The SAFOD drill hole, located 14 km northwest of Parkfield where the measured creep rate is 25 mm/yr [Titus *et al.*, 2006], crossed the active trace of the San Andreas fault at -2.7 km depth ($\sim 112^\circ\text{C}$). Two creeping strands were identified based on deformation of the steel casing lining the main drill hole and both were successfully sampled during subsequent coring operations. In marked contrast to the quartzofeldspathic sedimentary rock units adjoining them, the creeping traces are 1.6 and 2.6 m wide zones of saponite \pm corrensite-rich clayey gouge [Moore and Rymer, 2012] with porphyroclasts of serpentinite and sedimentary rock. The gouge of the main creeping strand contains ~ 27 wt% MgO, obtained by whole-rock XRF analysis [Bradbury *et al.*, 2011]. At the surface, a narrow tectonic shear zone of serpentinite extends for several kilometers within the fault zone northwest of the drill site. Where visible in outcrop, the sheared contact of serpentinite with the sedimentary wall rocks is marked by saponite-rich gouge identical to that found at depth [Moore and Rymer, 2012]. Moore and Rymer [2012] concluded that the surface outcrops of serpentinite connect with one or both of the creeping strands, which consist of more highly altered, sheared serpentinite. In effect, the tectonically entrained serpentinite at the SAFOD locality corresponds to the sample configuration used in this study (Figure 1b), and the gouges represent the experiment in Figure 10 run for a geologic time span at temperatures within the stability range of saponite. Based on the timing of major changes in

the nature and orientations of off-fault geologic structures, Titus *et al.* [2011] estimated that the fault creep initiated 2–2.5 Myr ago along the central San Andreas fault, and they linked the change to the tectonic incorporation of serpentinite into the fault.

[43] The forceful injection of serpentinite into overlying rocks, proposed to occur at SAFOD, is a common mode of emplacement of serpentinite [Lockwood, 1971, 1972]. Both active [e.g., 2010 Ohlin *et al.*, 2010] and inactive [e.g., Dickinson, 1966; Page *et al.*, 1999] faults have provided pathways facilitating the upward migration of the serpentinite. Despite its common occurrence, the cause of the emplacement has been disputed. The relatively low density of serpentinite compared to that of the overlying rock units is typically cited as a factor promoting this process. However, Phipps [1984] argued that the density contrast between serpentinite and typical crustal rocks is too small to be effective. Furthermore, based on their strength experiments on serpentinitized ultramafic rock, Raleigh and Paterson [1965] concluded that tectonic emplacement of serpentinite was unlikely to occur at temperatures below $\sim 300^\circ\text{C}$, because of its high strength. Cowan and Mansfield [1970] and Saleeby [1984], among others, noted that in many cases tectonically emplaced serpentinites are intensively sheared along the margins, while the interiors have a more massive appearance. They inferred that the sheared-serpentinite margins somehow act as “lubricants,” facilitating low-temperature tectonic transport of the entire mass. Our results suggest that weakening of serpentinite along its contact with crustal rocks may be the source of that lubricating effect.

5.2.2. Faults Within Serpentine

[44] The behavior of crustal faults within serpentinite bodies may vary, depending on the chemistry of the pore fluids in the fault zone. In one end-member case, the fault is an open system for fluid flow, and fluid chemistry largely reflects equilibration with an external, crustal rock reservoir. Retention of the crustal signature in groundwater chemistry will be favored by high groundwater flow rates and by passage through relatively small ultramafic masses. Such faults are likely to be characterized by weakening and aseismic slip. They would also provide the best environment for serpentine minerals rather than a metasomatic mineral assemblage to precipitate as the end product of a solution-transfer mechanism.

[45] Possible examples have been described by Andreani *et al.* [2005] and Bellot [2008]. Andreani *et al.* [2005] studied a shear zone developed within a kilometer-scale serpentinite lens along a segment of the Santa Ynez fault in California. They concluded that elongate chrysotile fibers in the serpentinite gouge within the shear formed by continuous syntectonic crystallization. Their model involved dissolution of serpentine minerals along R_1 and Y subsidiary shears and crystallization of the chrysotile in the gouge in between the shears, resulting in aseismic slip. Bellot [2008] examined a serpentinitized ultramafic body, approximately 170 m \times 250 m in horizontal dimensions, enclosed within amphibolites in a continental shear zone in the Maures Massif, France. He described crack-seal chrysotile veins that he considered to be the product of solution-transfer processes.

[46] As the size of the faulted ultramafic body increases, so does the potential for fluid chemistry within the fault to be controlled by the enclosing ultramafic rocks. Candidates

would be the ultramafic bodies whose groundwaters, discharged from springs and seeps, have extremely high pH and ultrabasic chemistry [Barnes and O'Neil, 1969; Barnes et al., 1972]. In the end-member case, the frictional behavior of serpentinite documented in previous studies for ultramafic chemical systems [e.g., Reinen et al., 1991, 1992, 1994; Moore et al., 1997, 2004] should be applicable.

6. Concluding Remarks

[47] These experiments demonstrate that the contrast in rock chemistry will promote an immediate stabilization of shear and dramatic weakening of serpentinite faulted against quartzose crustal rocks. This behavior occurs at depths that typically are within the seismogenic zone of continental crust. Our results provide a possible explanation for the common occurrence of creep in faults of the San Andreas system in central and northern California that are associated with serpentinite. Knowledge of the depth distribution of serpentinite along such faults thus potentially contributes to the evaluation of seismic hazard.

[48] The juxtaposition of silica-undersaturated ultramafic rocks against quartz-rich rocks that was examined in this study represents an extreme case of chemical incompatibility. However, it is possible that other combinations of rock types will also lead to chemically induced modifications of fault behavior. This possibility should be tested in future laboratory investigations at hydrothermal conditions.

Appendix A: Procedure for Determining Velocity Dependence of Strength and Additional Data for Serpentine

[49] At each velocity step of the velocity-stepping experiments in Figures 5b and 7, the change in μ was measured and the error estimated. Seal friction is a function

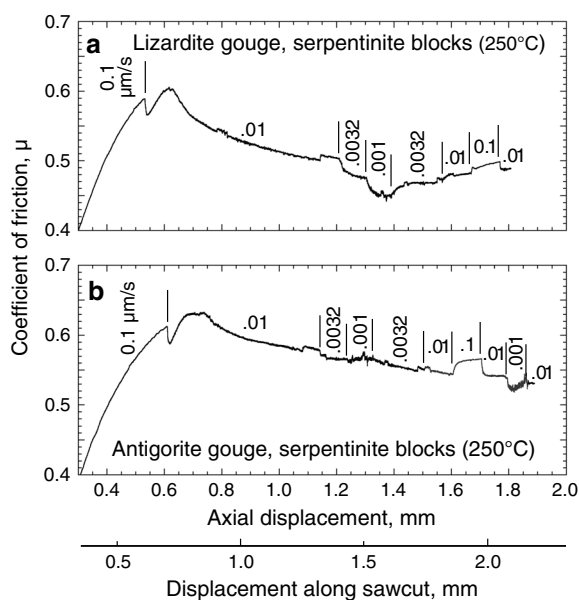


Figure A1. Velocity-stepping experiments at 250°C on (a) lizardite-serpentine and (b) antigorite-serpentine gouges sheared between driving blocks of serpentinite in Cu jackets. Measured values of $\Delta\mu_{ss}/\Delta\ln V$ are included in Figure 8.

of velocity, and the velocity dependence of seal friction was checked at the beginning of each experiment by means of a velocity step that was made before the piston reached the sample. For the experiments in this study, a correction of $\Delta\mu_{seal}/\Delta\ln V=0.0007$ was subtracted from the raw data. An additional correction to account for the velocity dependence of the Cu and Ag jacket strengths was made, as determined from calibration tests on the jacket stocks. Both the Ag and Cu jacket corrections are $\Delta\mu_{jacket}/\Delta\ln V=0.0010$, and this value was also subtracted from the data, as appropriate. In contrast, calibration experiments indicated no velocity dependence of Pb-jacket strength.

[50] Two additional experiments using serpentinite driving blocks were run at 250°C, one each on the antigorite- and lizardite-rich gouges (Figure A1), to provide velocity data for comparison with the data from experiments presented in Figures 5b and 7b. The velocity data from Figure A1, determined using the procedure described above, are included in Figure 8.

[51] **Acknowledgments.** We thank R. Oscarson for his help with the SEM work, and N. Beeler, R. Evarts, E. Rutter, and M. Takahashi for helpful manuscript reviews.

References

- Allen, C. R. (1968), The tectonic environments of seismically active and inactive areas along the San Andreas fault system, in *Proceedings of Conference on Geologic Problems of San Andreas Fault System*, edited by W. R. Dickinson, and A. Grantz, Stanford Univ. Publ. Geol. Sci., 11, pp. 70–80, Stanford University, Stanford, Calif.
- Andreani, M., A.-M. Boullier, and J.-P. Gratier (2005), Development of schistosity by dissolution-crystallization in a Californian serpentinite gouge, *J. Struct. Geol.*, 27, 2256–2267.
- Bales, R. C., and J. J. Morgan (1985), Dissolution kinetics of chrysotile at pH 7 to 10, *Geoch. Cosmoch. Acta*, 49, 2281–2288.
- Barnes, I., and J. R. O'Neil (1969), The relationship between fluids in some fresh alpine-type ultramafics and possible modern serpentinization, Western United States, *Geol. Soc. Am. Bull.*, 80(10), 1947–1960.
- Barnes, I., J. B. Rapp, and J. R. O'Neil (1972), Metamorphic assemblages and the direction of flow of metamorphic fluids in four instances of serpentinization, *Contrib. Mineral. Petrol.*, 35, 263–276.
- Bellot, J.-P. (2008), Natural deformation related to serpentinization of an ultramafic inclusion within a continental shear zone: The key role of fluids, *Tectonophysics*, 449, 133–144.
- Blanpied, M. L., D. A. Lockner, and J. D. Byerlee (1995), Frictional slip of granite at hydrothermal conditions, *J. Geophys. Res.*, 100(B7), 13,045–13,064.
- Bos, B., and C. J. Spiers (2001), Experimental investigation into the microstructural and mechanical evolution of phyllosilicate-bearing fault rock under conditions favoring pressure solution, *J. Struct. Geol.*, 23, 1187–1202.
- Bradbury, K. K., J. P. Evans, J. S. Chester, F. M. Chester, and D. L. Kirschner (2011), Lithology and internal structure of the San Andreas fault at depth based on characterization of phase 3 whole-rock core in the San Andreas Fault Observatory at Depth (SAFOD) borehole, *Earth Planet. Sci. Lett.*, 310, 131–144, doi:10.1016/j.epsl.2011.07.020.
- Chernak, L. J., and G. Hirth (2010), Deformation of antigorite serpentinite at high temperatures and pressures, *Earth Planet. Sci. Lett.*, 296, 23–33, doi:10.1016/j.epsl.2010.04.035.
- Chéry, J., M. D. Zoback, and S. Hickman (2004), A mechanical model of the San Andreas Fault and SAFOD Pilot Hole stress measurements, *Geophys. Res. Lett.*, 31, L15S13, doi:10.1029/2004GL019521.
- Chester, F. M. (1995), A rheologic model for wet crust applied to strike-slip faults, *J. Geophys. Res.*, 100(B7), 13,033–13,044.
- Chester, F. M., and N. G. Higgs (1992), Multimechanism friction constitutive model for ultrafine quartz gouge at hypocentral conditions, *J. Geophys. Res.*, 97(B2), 1859–1870.
- Coleman, R. G. (1961), Jadeite deposits of the Clear Creek area, New Idria district, San Benito County, California, *J. Petrol.*, 2(2), 209–247.
- Coleman, R. G. (1967), Low-temperature reaction zones and alpine ultramafic rocks of California, Oregon, and Washington, *U. S. Geol. Survey Bull.*, 1247, 49 pp.

- Cowan, D. S., and C. F. Mansfield (1970), Serpentine flows on Joaquin Ridge, southern Coast Ranges, California, *Geol. Soc. Am. Bull.*, *81*, 2615–2628.
- Dickinson, W. R. (1966), Table Mountain serpentinite extrusion in California Coast Ranges, *Geol. Soc. Am. Bull.*, *77*, 451–472.
- Ellis, A. C., E. H. Rutter, K. H. Brodie, and J. Mecklenburgh (2010), Effect of hydrothermally produced talc upon fault strength, *Eos Trans AGU*, *91*, Fall Meet. Suppl., Abstract T41B-2116.
- Frantz, J. D., and H. K. Mao (1976), Bimetasomatism resulting from intergranular diffusion: I. A theoretical model for monomineralic reaction zone sequences, *Am. J. Sci.*, *276*(7), 817–840.
- Frantz, J. D., and H. K. Mao (1979), Bimetasomatism resulting from intergranular diffusion: II. Prediction of multiminerallitic zone sequences, *Am. J. Sci.*, *279*(3), 302–323.
- Fulton, P. M., D. M. Saffir, R. N. Harris, and B. A. Bekins (2004), Re-evaluation of heat flow data near Parkfield, CA: Evidence for a weak San Andreas fault, *Geophys. Res. Lett.*, *31*, L15S15, doi:10.1029/2003GL019378.
- Galehouse, J. S., and J. J. Lienkaemper (2003), Inferences drawn from two decades of alignment array measurements of creep on faults in the San Francisco Bay region, *Seismol. Soc. Am. Bull.*, *93*, 2415–2433, doi:10.1785/0120020226.
- Hanna, W. F., R. D. Brown Jr., D. C. Ross, and A. Griscom (1972), Aeromagnetic reconnaissance and generalized geologic map of the San Andreas fault between San Francisco and San Bernardino, California, *U. S. Geol. Surv. Geophys. Invest. Map*, GP-815, scale 1:250,000.
- Hickman, S., and M. Zoback (2004), Stress orientations and magnitudes in the SAFOD pilot hole, *Geophys. Res. Lett.*, *31*, L15S12, doi:10.1029/2004GL020043.
- Hirauchi, K.-I., S. A. M. den Hartog, and C. J. Spiers (2013), Weakening of the slab-mantle wedge interface induced by metasomatic growth of talc, *Geology*, *41*(1), 75–78, doi:10.1130/G33552.1.
- Irwin, W. P. (1990), Geology and plate-tectonic development, in *The San Andreas Fault System, California*, edited by R. E. Wallace, U. S. Geol. Surv. Prof. Pap., 1515, pp. 61–80.
- Irwin, W. P., and I. Barnes (1975), Effect of geologic structure and metamorphic fluids on seismic behavior of the San Andreas fault system in central and northern California, *Geology*, *3*(12), 713–716.
- Jahns, R. H. (1967), II. Serpentinities of the Roxbury district, Vermont, in *Ultramafic and Related Rocks*, edited by P. J. Wyllie, and E. Robert, pp. 137–160, Krieger Publishing Company, New York.
- Koons, P. O. (1981), A study of natural and experimental metasomatic assemblages in an ultramafic-quartzofeldspathic system from the Haast Schist, South Island, New Zealand, *Contrib. Mineral. Petrol.*, *78*, 189–195.
- Krauskopf, K. B. (1967), *Introduction to Geochemistry*, McGraw-Hill Book Company, New York.
- Lin, F.-C., and C. V. Clemency (1981), The dissolution kinetics of brucite, antigorite, talc, and phlogopite at room temperature and pressure, *Am. Mineral.*, *66*, 801–806.
- Lockner, D. A., C. Morrow, D. Moore, and S. Hickman (2011), Low strength of deep San Andreas Fault gouge from SAFOD core, *Nature*, *472*, 82–85, doi:10.1038/nature09927.
- Lockwood, J. P. (1971), Sedimentary and gravity-slide emplacement of serpentinite, *Geol. Soc. Am. Bull.*, *82*, 919–936.
- Lockwood, J. P. (1972), Possible mechanism for the emplacement of Alpine-type serpentinites, *Geol. Soc. Am. Mem.*, *132*, 273–287.
- Luce, R. W., R. W. Bartlett, and G. A. Parks (1972), Dissolution kinetics of magnesium silicates, *Geoch. Cosmoch. Acta*, *36*, 35–50.
- McFarland, F. S., J. J. Lienkaemper, and S. J. Caskey (2009), Data from theodolite measurements of creep rates on San Francisco Bay region faults, California, 1979–2011, *U. S. Geol. Surv. Open File Rep.*, 2009-1119, 18 pp., <http://pubs.usgs.gov/of2009/1119/>, last accessed.
- Moore, D. E., and D. A. Lockner (2007), Comparative deformation behavior of minerals in serpentinized ultramafic rock: Application to the slab-mantle interface in subduction zones, *Int. Geol. Rev.*, *49*, 401–415, doi:10.2747/0020-6814.49.5.401.
- Moore, D. E., and D. A. Lockner (2008), Talc friction in the temperature range 25°–400°C: Relevance for fault-zone weakening, *Tectonophysics*, *449*, 120–132, doi:10.1016/j.tecto.2007.11.039.
- Moore, D. E., and D. A. Lockner (2011), Frictional strengths of talc-serpentinite and talc-quartz mixtures, *J. Geophys. Res.*, *116*, B01403, doi:10.1029/2010JB07881.
- Moore, D. E., D. A. Lockner, R. Summers, J. D. Byerlee, and S. Ma (1996a), Sample characterizations and strength measurements of serpentinite gouges, *U.S. Geol. Surv. Open File Rep.*, 96-702, 88 pp.
- Moore, D. E., D. A. Lockner, R. Summers, S. Ma, and J. D. Byerlee (1996b), Strength of chrysotile-serpentinite gouge under hydrothermal conditions: Can it explain a weak San Andreas fault?, *Geology*, *24*(11), 1041–1044.
- Moore, D. E., C. A. Morrow, and J. Byerlee (1987), Fluid-rock alteration and fracture development in “crystalline” rock types, *U.S. Geol. Surv. Open File Rep.*, 87-279, 53 pp.
- Moore, D. E., D. A. Lockner, S. Ma, R. Summers, and J. D. Byerlee (1997), Strengths of serpentinite gouges at elevated temperatures, *J. Geophys. Res.*, *102*, 14,787–14,801.
- Moore, D. E., D. A. Lockner, H. Tanaka, and K. Iwata (2004), The coefficient of friction of chrysotile gouge at seismogenic depths, *Int. Geol. Rev.*, *46*, 385–398, doi:10.2747/0020-6814.46.5.385.
- Moore, D. E., D. A. Lockner, and D. A. Ponce (2010), Anomalous low strength of serpentinite sheared against granite and implications for creep on the Hayward and Calaveras Faults, in *Proceedings of the Third Conference on Earthquake Hazards in the Eastern San Francisco Bay Area*, edited by K. Knudsen et al., California Geol. Surv. Spec. Rep., 219, pp. 101–113, California Geological Survey (Dept. of Natural Resources), Sacramento, Calif.
- Moore, D. E., and M. J. Rymer (2012), Correlation of clayey gouge in a surface exposure of serpentinite in the San Andreas Fault with gouge from the San Andreas Fault Observatory at Depth (SAFOD), *J. Struct. Geol.*, *38*, 51–60, doi:10.1016/j.jsg.2011.11.014.
- Mori, Y., T. Nishiyama, and T. Yanagi (2007), Chemical mass balance in a reaction zone between serpentinite and metapelites in the Nishisonogi metamorphic rocks, Kyushu, Japan: Implications for devolatilization, *Island Arc*, *16*, 28–39, doi:10.1111/j.1440-1738.2007.00556.x.
- Ohlin, H. N., R. J. McLaughlin, B. C. Moring, and T. L. Sawyer (2010), Geologic map of the Bartlett Springs Fault Zone in the vicinity of Lake Pillsbury and adjacent areas of Mendocino, Lake, and Glenn Counties, California, *U. S. Geol. Surv. Open File Rep.*, 2010-1301, 32 pp.
- Page, B. M., L. A. DeVito, and R. G. Coleman (1999), Tectonic emplacement of serpentinite southeast of San Jose, California, *Int. Geol. Rev.*, *41*, 494–505.
- Phipps, S. P. (1984), Ophiolitic olistostromes in the basal Great Valley sequence, Napa County, northern Coast Ranges, in *Mélanges: Their Nature, Origin and Significance*, edited by L. A. Raymond, Geol. Soc. Am. Spec. Pap., 198, 103–126.
- Raleigh, C. B., and M. S. Paterson (1965), Experimental deformation of serpentinite and its tectonic implications, *J. Geophys. Res.*, *70*, 3965–3985.
- Reinen, L. A., and T. E. Tullis (1995), Microstructural evidence of strain localization and distributed strain in serpentinite friction experiments, *Eos Trans AGU*, 76(46), Fall Meet. Suppl., F566.
- Reinen, L. A., J. D. Weeks, and T. E. Tullis (1991), The frictional behavior of serpentinite: Implications for aseismic creep on shallow crustal faults, *Geophys. Res. Lett.*, *18*, 1921–1924.
- Reinen, L. A., T. E. Tullis, and J. D. Weeks (1992), Two-mechanism model for frictional sliding of serpentinite, *Geophys. Res. Lett.*, *19*, 1535–1538.
- Reinen, L. A., J. D. Weeks, and T. E. Tullis (1994), The frictional behavior of lizardite and antigorite serpentinites: Experiments, constitutive models, and implications for natural faults, *Pure Appl. Geophys.*, *143*, 317–358.
- Rutter, E. H., and D. H. Mainprice (1978), The effect of water on stress relaxation of faulted and unfaulted sandstone, *Pure Appl. Geophys.*, *116*, 634–654.
- Rutter, E. H., and D. H. Mainprice (1979), On the possibility of slow fault slip controlled by a diffusive mass transfer process, *Gerlands Beitr. Geophysik. Leipzig*, *88*, 154–162.
- Saleeby, J. B. (1984), Tectonic significance of serpentinite mobility and ophiolitic mélange, in *Mélanges: Their Nature, Origin and Significance*, edited by L. A. Raymond, Geol. Soc. Am. Spec. Pap., 198, 153–168.
- Sanford, R. F. (1982), Growth of ultramafic reaction zones in greenschist to amphibolite facies metamorphism, *Am. J. Sci.*, *282*, 5543–616.
- Scott, D. R., D. A. Lockner, J. D. Byerlee, and C. G. Sammis (1994), Triaxial testing of Lopez fault gouge at 150 MPa mean effective stress, *Pure Appl. Geophys.*, *142*, 749–775.
- Tembe, S., D. A. Lockner, and T.-F. Wong (2010), Effect of clay content and mineralogy on frictional sliding behavior of simulated gouges: Binary and ternary mixtures of quartz, illite, and montmorillonite, *J. Geophys. Res.*, *115*, B03416, doi:10.1029/2009JB006383.
- Titus, S. J., C. DeMets, and B. Tikoff (2006), Thirty-five-year creep rates for the creeping segment of the San Andreas Fault and the effects of the 2004 Parkfield earthquake: Constraints from alignment arrays, continuous global positioning system, and creepmeters, *Seismol. Soc. Am. Bull.*, *96* (4B), S250–S268, doi:10.1785/0120050811.
- Titus, S. J., M. Dyson, C. DeMets, B. Tikoff, F. Rolandone, and R. Bürgmann (2011), Geologic versus geodetic deformation adjacent to the San Andreas fault, central California, *Geol. Soc. Am. Bull.*, *123*, 794–820, doi:10.1130/B30150.1.
- Welton, J. E. (1984), *SEM Petrology Atlas, AAPG Methods in Exploration Series*, 4, AAPG, Tulsa, Oklahoma.
- Williams, C. F., F. V. Grubb, and S. P. Galanis, Jr. (2004), Heat flow in the SAFOD pilot hole and implications for the strength of the San Andreas Fault, *Geophys. Res. Lett.*, *31*, L15S14, doi:10.1029/2003GL019352.
- Zoback, M., S. Hickman, and W. Ellsworth (2011), Scientific drilling into the San Andreas Fault zone—An overview of SAFOD’s first five years, *Sci. Drill.*, *11*, 14–28, doi:10.2204/iopd.sd.11.02.2011.